

Decoherence and single electron charging in an electronic Mach-Zehnder interferometer

L. V. Litvin,^{1,*} H.-P. Tranitz,¹ W. Wegscheider,¹ and C. Strunk¹

¹ Institut für experimentelle und angewandte Physik, Universität Regensburg, D-93040 Regensburg, Germany

We investigate the temperature and voltage dependence of the quantum interference in an electronic Mach-Zehnder interferometer using edge channels in the integer quantum-Hall-regime. The amplitude of the interference fringes is significantly smaller than expected from theory; nevertheless the functional dependence of the visibility on temperature and bias voltage agrees very well with theoretical predictions. Superimposed on the Aharonov-Bohm (AB) oscillations, a conductance oscillation with six times smaller period is observed. The latter depends only on gate voltage and not on the AB-phase, and can be interpreted as single electron charging of the edge channels.

PACS numbers: 73.23.-b, 73.23.Ad, 73.63.Nm

Electron interferences in mesoscopic conductors manifest itself in conductance oscillations which are h/e periodic in the magnetic field B [1]. In conventional metals the visibility ν_I of these Aharonov-Bohm (AB) oscillations typically amounts to $\nu_I = G_0/G \simeq 10^{-4}$, where G is the conductance of the sample and $G_0 = 2e^2/h$ the conductance quantum. The visibility can be enhanced to $\nu_I \simeq 0.1$ by reducing the number of conductance channels, e.g. in nanostructures based on two-dimensional electron systems [2, 3] containing only a small number of conductance channels. Recently an electronic analogue [4] of the well known optical Mach-Zehnder interferometer (MZI) was realized, which employs the one-dimensional edge channels in the integer quantum Hall regime [5]. In these devices single channel interference can be realized, while backscattering processes are suppressed. This results in measured visibilities up to $\nu_I \simeq 0.6$. Such devices open a path for the realization of fundamental two-particle interference experiments in the spirit of Hanbury-Brown and Twiss [6], as recently proposed [7].

We have realized MZIs similar to those in Ref. 5. A quantum point contact (QPC) is used to partition an edge channel leaving contact S into two paths. After propagation of the edge channel along the inner and outer edge of an ring-shaped mesa, the two paths are brought to interference at a second QPC, resulting in two output channels D1 and D2 of the interferometer (see Fig. 1). The phase of the two partial waves can be changed both by magnetic field and by an electrostatic gate G. The measured visibility is much smaller than expected from theory [8] and reported in Ref. 5. Despite this quantitative disagreement, the functional dependence of ν on T and V_{bias} fits very well the simple model of Ref. 8. In addition to the AB-oscillations we found another type of conductance oscillations. It has a significantly smaller period in gate voltage when compared to the AB period

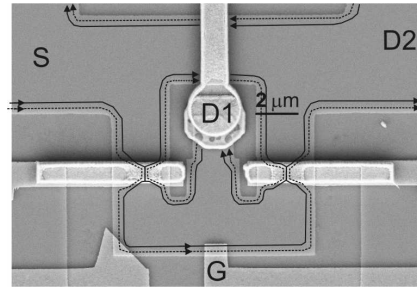


FIG. 1: SEM image of Mach-Zehnder interferometer with the scheme of edge states for filling factor 2. The inner edge channel (full line) is split into two branches using QPCs.

and is attributed to single electron charging of the section of the edge states confined between two QPCs.

The mesa was prepared through wet etching of a modulation doped GaAs/Ga_xAl_{1-x}As heterostructure containing a two-dimensional electron system (2DES) 90 nm below the surface. At 4 K, the unpatterned 2DES density and mobility were $n=2.0 \times 10^{15} \text{ m}^{-2}$ and $\mu=206 \text{ m}^2/(\text{V s})$, respectively. Using standard electron beam lithography techniques, we prepared split gates connected by air bridges, defining QPCs of 500 nm length and 220 nm gap width. The measurements were performed in a dilution refrigerator with two stages of copper powder filters at bath temperature and at 100 mK. The currents at contacts D1 and D2 were measured using a lock-in technique with an ac excitation voltage (1 kHz) of 10–16 μV applied to contact S.

To characterize the samples, we first verified that the current through contact D1 goes to zero when the filling factor ν approaches 1 or 2 (see Fig. 2). This implies a complete suppression of backscattering between the edge channels at the opposite edges of the mesa (Fig. 2, curve D1). The sum of both detector currents, $I_{D1} + I_{D2}$ shows quantized current (conductance) levels which allows us to determine the value of ν . From the position of the minima in current D1 (marked by vertical arrows in Fig. 2) at magnetic fields $B_\nu = \frac{n\hbar}{\nu e}$ for $\nu = 3, 4, 6$ we determine an electron density $n=1.7 \times 10^{15} \text{ m}^{-2}$ which is 15 % smaller

*Permanent address: Institute of Semiconductor Physics, 630090, Novosibirsk, Russia

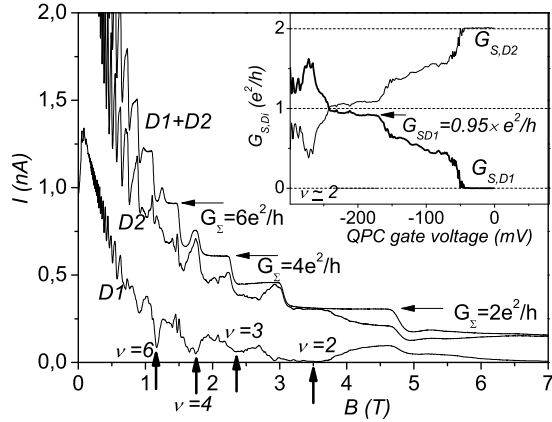


FIG. 2: The currents collected by D1, D2 and their sum as function of magnetic field at $V_{\text{bias}} = 4 \mu\text{V}$ and $T=25 \text{ mK}$, when both QPCs are open. The thick vertical arrows show magnetic fields corresponding to the indicated filling factors; the horizontal arrows label conductance level. Inset: two point conductance between contacts S, D1 and S,D2 as function of gate voltage at one of the QPCs for $B = 3.26 \text{ T}$; the second QPC is open.

than that of the unpatterned 2DES because of the depletion near the mesa edges. If we apply a negative voltage at one of the QPCs at $\nu \approx 2$, the inner edge channel starts to split into two branches flowing into D1 and D2. When the QPC is pinched off the current will be completely redirected from D2 into D1. Then, the conductance $G_{S,D1}$ will be close to $2e^2/h$ (inset to Fig.2). In our experiment the conductance $G_{S,D1}$ at the plateau reaches about 95% of (e^2/h) . This implies a high transmission of the miniature ohmic contact D1, reflecting only 5% of the incident current back into the edge channel.

To observe interference both QPCs were tuned to transmission 1/2 for the inner edge channel (full line at Fig.1). The currents at D1 and D2 as a function of gate voltage V_G are shown at Fig.3(a), 3(b) respectively. Current conservation requires that the oscillations detected in D1 and D2 should go in antiphase and sum up to a constant value [Fig.3(c)]. Two periods of oscillation are seen in these traces. The amplitude of the small period oscillations is not constant and shows a beating-like pattern. Fourier analysis reveals two periods of 0.71 and 0.80 mV for the small period oscillations and a period of 5.1 mV for the large period oscillations [Fig.3(d)]. Since the AB-period h/e amounts to $78 \mu\text{T}$, a direct measurement of the magnetic field dependence of the interference pattern requires control of the magnetic field at a level below 10^{-6} . Since this is difficult to achieve, we have exploited the gradual decay of the magnetic field in persistent mode at a rate of about $20 \mu\text{T}/\text{h}$. In this way the time delay between successive traces can be translated into changes of B . In Fig. 4 we show a sequence of gate

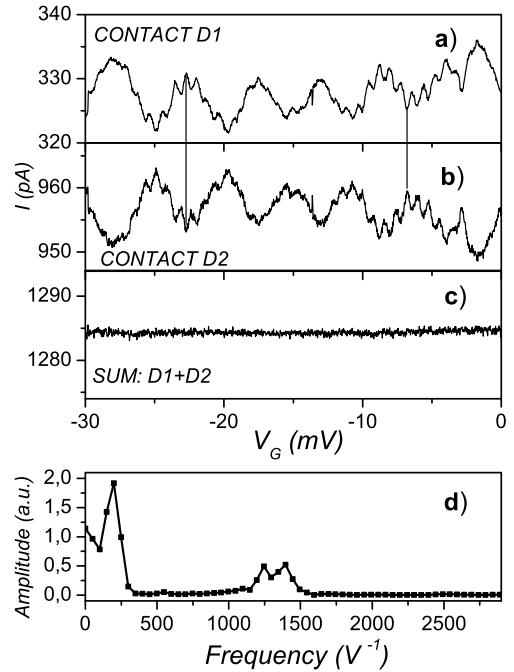


FIG. 3: The currents collected by D1 (a), D2 (b), their sum (c) as function of gate G voltage at $T=25 \text{ mK}$, $B=3.27 \text{ T}$ ($\nu=2.14$). (d) Typical Fourier spectrum of oscillations.

sweeps recorded with time delays of 10 min. The large period oscillations shift linearly with time delay to the left, indicating that these oscillations are of the expected Aharonov-Bohm type. Besides the regular oscillations we observed an occasional switching of the phase of the large period oscillation by $\simeq \pi$ (see, e.g., dashed line in Fig. 4). We attribute these events to slow random transitions of charged impurities between two metastable states. The maximum visibility for the observed AB oscillations was 1.5%. In contrast to these, the small period oscillations do not shift with time and thus do not depend on magnetic field (Fig.4). This fact points towards an electrostatic origin of this effect.

We now discuss the decay of the oscillation amplitude with temperature and bias voltage. The temperature dependence of the amplitude for both types of oscillations is displayed in Fig. 5. The amplitude of the AB oscillation was averaged first over a few oscillations in a single trace and than over four sweeps taken at each temperature. The amplitude of the small period oscillations was calculated by integrating the Fourier spectrum within a region including both high frequency peaks, i.e. from 1200 to 1450 V^{-1} . From Fig. 5 we can infer a characteristic energy $E_C \simeq 9 \mu\text{eV}$ (corresponding to $T_C=100 \text{ mK}$) related to the small period oscillation. The peak at higher frequency (1400 V^{-1}) decays more rapid than the peak at 1250 V^{-1} both with increasing temperature (inset in Fig. 5) and bias voltage.

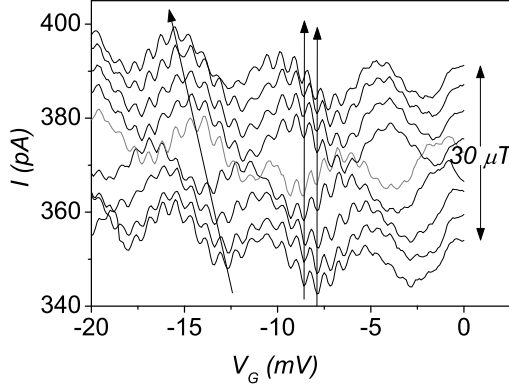


FIG. 4: The time evolution of oscillation at $T=25$ mK, $B=3.27$ T ($\nu=2.14$) indicated by the gradual decay of magnetic field in persistant mode. Successive traces are recorded with 10 min time delay (traces are vertically shifted for clarity by 5 pA). The arrow indicate the progressing recording time and the time shift of the oscillations. The gray curve in the middle displays a phase lapse by π at $V_G=-11$ mV and separates two trains with linear phase evolution.

According to Ref. 8 the visibility of the AB oscillations $\nu_I = (I_{max} - I_{min})/(I_{max} + I_{min})$ decays with the temperature or voltage as

$$\nu_I = \frac{1}{2} \frac{4\pi k_B T}{eV} \left[\sinh \left(\frac{k_B T \pi}{E_b} \right) \right]^{-1} \left| \sin \left(\frac{eV}{2E_b} \right) \right|. \quad (1)$$

The prefactor $1/2$ corresponds to QPC transmission probabilities $T_A = T_B = 1/2$. The T - and V_{bias} -dependence scales with another characteristic energy E_b . E_b determines the phase an electron acquires traversing the asymmetric interferometer with a difference ΔL in path length between the two interferometer arms. An electron at energy E above the Fermi energy E_F collects a phase difference $\Delta\phi(E) = \Delta\phi(E_F) + E/E_b$, where $E_b \approx \hbar v_D/(\Delta L)$ and v_D being the drift velocity. The energy dependence of this phase difference smears the interference pattern when the interfering electrons are spread over energy ranges $k_B T$ and E_{bias} . This is in complete analogy to the interference of a polychromatic light beam in optics. Equation 1 perfectly reproduces the shape of the measured curves (Fig.6) but not the absolute value of the visibility. The latter is 80 times smaller in our experiment.

The values of $E_b \simeq 18$ μeV extracted from the fit of the T - and V_{bias} -dependence of Eq. 1 to the data coincide within 3% accuracy. The theory assumes a dc voltage bias, while we used an ac bias in the experiment. Averaging over the ac bias window results in the solid line in Fig. 6(b), which is again in complete agreement with the data.

Next we connect the energy scales E_C and E_b with the geometric parameters of our device. From the location

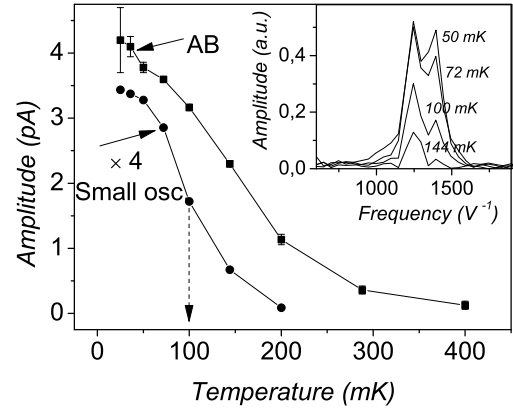


FIG. 5: Measured amplitude of Aharonov-Bohm (squares) and small period oscillations (open circles) as function of temperature. Inset: Evolution of the spectrum of the small oscillations with temperature.

of the inner edge channel we can deduce the path difference ΔL between the two interferometer arms, which determines E_b . Taking into account the depletion region at the mesa edge we estimate the distance between the mesa edge and the location of inner edge channel. Our estimate is based on the electron density extracted from the positions of current minima at integer filling factor in D1 (see Fig.2) for the MZIs with the arm width of 2.5 and 1.7 μm. Using the edge reconstruction model [10], we find a depletion length of $2l=180$ nm, a distance between the mesa edge and the center of the incompressible strip $x_1=150$ nm (for $\nu=2$) and the width of incompressible strip $a_1=45$ nm. This results in a distance $l + x_1 + a_1/2 = 260$ nm between the mesa edge and the inner edge strip for our interferometer, implying that the length of the two interferometer arms differs by about $\Delta L=2.0$ μm. The known E_b and ΔL yield the drift velocity of 5×10^4 m/s which agrees well with other estimates [11] for the edge state regime.

The question remains, why the measured visibility of the AB oscillations for our interferometer is so small. It can be seen from Fig. 6 that ν_I remains temperature dependent down to 50 mK, indicating that ν_I is not limited by a substantially elevated electron temperature. An intrinsic source of dephasing may result from the internal degrees of freedom of the QPC [12], which sensitively depend of the shape of the QPC potential. In our case the QPCs consist of rather long (500 nm) and narrow (200 nm) channels, which are quite different from an ideal saddle point potential. On the other hand, the good agreement of the shape of the decay of ν with theory seems to point towards a temperature independent source of dephasing.

In earlier experiments, a very high interference visibility of 60% was reported [5, 9]. This value rapidly dropped down to 1% when increasing the temperature

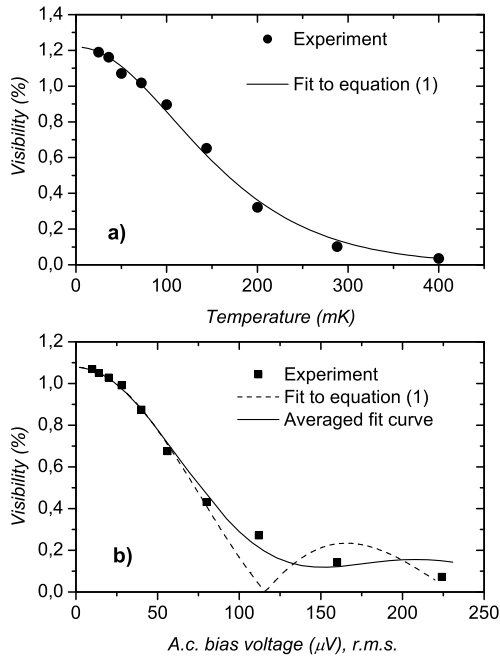


FIG. 6: Visibility decay as function of (a) temperature ($V_{bias} = 16 \mu\text{V}$, r.m.s.) and (b) voltage ($T = 25 \text{ mK}$). In (b) fitting was carried out in the V_{bias} -range $0 \div 80 \mu\text{V}$.

from 20 to 100 mK, indicating a relevant energy scale E_b even smaller than in our experiment. A satisfactory agreement between these experiments with simple theoretical models [8] is still lacking, since the data of Ref. 9 indicate a surprising independence of the visibility on the asymmetry between the interferometer arms.

We now return to the source of the small oscillations and their characteristic energy E_C . Partial Coulomb blockade in an open island may provide an electrostatic origin of the small oscillations. Such an island can be formed by the section of the edge strips between the two QPCs. In the Mach-Zehnder interferometer the oscillation is detected not due to backscattering like for a usual quantum dot but by redistributing current between D1 and D2. When one of the QPCs of the MZI is set to half transmission only a synchronous change of transmission for two QPCs both in-phase and antiphase

can cause the substantial current redistribution. This requires that the charging object has to have a spacial extension from one QPC to the other. The edge strips are the likely candidates. The dominating contribution to their capacitance comes from the electrochemical capacitance $C = Le^2/(hv_F)$, rather than from the geometrical capacitance. Here L is the channel length, and v_F is the Fermi velocity. The length between the QPCs in our interferometer of $15 \mu\text{m}$ then corresponds to a total capacitance of 7 fF and an associated charging energy of $25 \mu\text{eV}$. Since our edge channels are rather open this value is suppressed by number fluctuations [13] according to $\tilde{E}_C \propto E_C \exp\left(-\frac{\pi^2 G}{4G_0}\right)$, which results in $\tilde{E}_C \approx 7 \mu\text{eV}$. This agrees well with the value $E_C \approx 9 \mu\text{eV}$ extracted from Fig. 5. The gate capacitance extracted from the voltage period of the small oscillations is 0.2 fF , which is close to the value of 0.6 fF obtained from the capacitor formula $C = \epsilon\epsilon_0 S/d$ with ϵ_0 - dielectric constant of GaAs, S - overlap area between gate G and mesa ($0.5 \mu\text{m}^2$) and d - depth of the 2DEG. The two peaks in the spectrum of the small period oscillations may result from two edge channels. The peak at higher frequency corresponds to the inner channel because it has larger spatial extension in the direction perpendicular to the edge [10]. The larger width may also be the reason for a higher capacitance of this channel, which could also explain its more rapid decay with increasing temperature or voltage.

In conclusion, we investigated single channel interference in electronic Mach-Zehnder interferometers and found a strong and unexpected decoherence. Although the absolute value of the measured visibility is a factor 80 smaller than expected, the functional form of its suppression by finite temperature, bias voltage and asymmetry of two interfering paths agrees well with a simple model. In addition, we found a second type of oscillations which appears to be of electrostatic origin. These can be consistently explained by single electron charging of the section of edge state channels confined between the quantum point contacts.

We thank, M. Heiblum, J. Weis, F. Marquardt, S. Ludwig and J. Kotthaus for stimulating discussions. This work was supported by the Deutsche Forschungsgemeinschaft in the framework of SFB631 "Solid state quantum information processing".

-
- [1] For a review see e.g., S. Washburn and R. A. Webb, Rep. Prog. Phys. **55**, 1311 (1992).
- [2] M. Casse, Z. D. Kvon, G. M. Gusev, E. B. Olshanetskii, L. V. Litvin, A. V. Plotnikov, D. K. Maude, and J. C. Portal, Phys. Rev. B **62**, 2624 (2000).
- [3] A. E. Hansen, A. Kristensen, S. Pedersen, C. B. Sorensen, and P. E. Lindelof, Phys. Rev. B **64**, 045327 (2001).
- [4] Seelig, G. and Büttiker M., Phys. Rev. B **64**, 245313 (2001).
- [5] Y. Ji, Y. Chung, D. Spinak, M. Heiblum, D. Mahalu, and H. Shtrikman, Nature **422**, 415 (2003).
- [6] R. Hanbury Brown and R. Q. Twiss, Nature **178**, 1046 (1956).
- [7] P. Samuelsson, E. V. Sukhorukov, and M. Büttiker, Phys. Rev. Lett. **92**, 026805-1 (2004).
- [8] V. S.-W. Chung, P. Samuelsson and M. Büttiker, Phys.

- Rev. B **72**, 125320-1 (2005).
- [9] I. Neder, M. Heiblum, Y. Levinson, D. Mahalu, and V. Umansky, cond-mat/0508024; Phys. Rev. Lett. **96**, 016804-1 (2006).
- [10] D. B. Chklovskii, B. I. Shklovskii, and L. I. Glazman, Phys. Rev. B **46**, 4026 (1992).
- [11] Komiyama S., Hirai H., Sasa S., Hiyamizu S., Phys. Rev. B **40**, 12566 (1989).
- [12] see, e.g., S. M. Cronenwett *et al.*, Phys. Rev. Lett. **88**, 226805 (2002) and the references therein.
- [13] Y. V. Nazarov, Phys. Rev. Lett. **82** 1245 (1999).